JCTC Journal of Chemical Theory and Computation

QM/MM Study of the NMR Spectroscopy of the Retinyl Chromophore in Visual Rhodopsin

José A. Gascón, Eduardo M. Sproviero, and Victor S. Batista*

Department of Chemistry, Yale University, P.O. Box 208107, New Haven, Connecticut 06520-8107

Received April 4, 2005

Abstract: The ^{1}H and ^{13}C nuclear magnetic resonance (NMR) spectra of the retinyl chromophore in rhodopsin are investigated by using quantum mechanics/molecular mechanics (QM/MM) hybrid methods at the density functional theory (DFT) B3LYP/6-31G*:Amber level of theory, in conjunction with the gauge independent atomic orbital (GIAO) method for the ab initio self-consistent-field (SCF) calculation of NMR chemical shifts. The study provides a first-principle interpretation of solid-state NMR experiments based on recently developed QM/MM computational models of rhodopsin and bathorhodopsin [Gascón, J. A.; Batista, V. S. *Biophys. J.* **2004**, *87*, 2931−2941]. The reported results are particularly relevant to the development and validation of atomistic models of prototypical G-protein-coupled receptors which regulate signal transduction across plasma membranes.

1. Introduction

G-protein-coupled membrane receptors (GPCRs) are macromolecules of great biological interest,[1−5] since they regulate signal transduction from the extracellular environment to the interior of every cell. The membrane glycoprotein rhodopsin is a prototypical GPCR present in rod cells of the retina.[4,6] Rhodopsin is particularly important in studies of GPCRs since it is the only member of the GPCR family whose crystal structure has been resolved at high-resolution. This paper investigates the ^{1}H NMR and ^{13}C NMR spectra of rhodopsin by using quantum mechanical/ molecular mechanics hybrid methods,[7−13] in conjunction with the gauge independent atomic orbital (GIAO) approach.[14,15] The study builds upon structural models recently developed in an effort to advance our understanding of the ligand binding site in a prototypical GPCR.[16]

Rhodopsin consists of 348-aa residues forming a bundle of seven transmembrane α-helices surrounding the 11-*cis* retinyl prosthetic group, a chromophore that is bound to Lys-296 via a protonated Schiff base (pSB) linkage,[17] stabilized by electrostatic interactions with the negatively charged Glu-113 counterion. Rhodopsin is responsible for triggering a signal transduction mechanism, through 11-cis/all-trans-isomerization of the retinyl ligand (see Figure 1), upon light absorption during the primary photochemical event.[17−20] The reaction produces bathorhodopsin in the ground electronic state,[21,22] with a high quantum yield within 200 fs, making it one of the fastest and most efficient photoreactions in nature.[1−3] The formation of the product bathorhodopsin is endothermic and stores approximately 50% of the photon energy.[20,23−25] The energy storage is required to promote thermal reactions in the protein bleaching sequence and in the subsequent transducin cycle. The underlying molecular rearrangements responsible for energy storage have been recently analyzed in terms of rigorous DFT QM/MM (molecular orbitals: molecular mechanics) (QM/MM-(MO:MM)) hybrid methods as applied to the refinement of high-resolution X-ray structures of bovine rhodopsin.[16]

There are currently four high-resolution structures of rhodopsin in the literature. The original 2.8 Å structure (PDB identifier 1F88)[26] is the first high-resolution structure of a GPCR revealing all the major features of the protein previously obtained from a variety of experimental data, including cryomicroscopy.[27] A refined model (PDB identifier 1HZX)[28] adds some amino acid residues not identified from the original work. A more recent structure (PDB identifier 1L9h) improves the resolution to 2.6 Å and resolves essential structural components of the chromophore binding site,

* Corresponding author e-mail: victor.batista@yale.edu.

10.1021/ct0500850 CCC: $30.25
Published on Web 06/03/2005

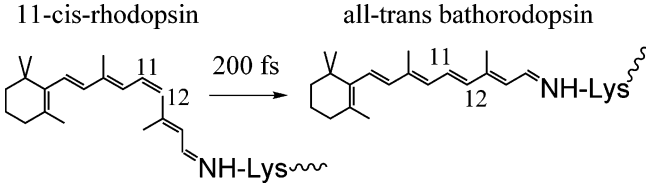

Figure 1. Photoisomerization of the retinyl chromophore in rhodopsin.

including two bound-water molecules next to the retinyl chromophore.[29] Finally, the most recent structure (PDB identifier 1U19) completely resolves the polypeptide chain at 2.2 Å resolution and provides further conformational details of the retinyl chromophore.[30] However, even with these breakthroughs in X-ray spectroscopy, the crystallographic resolution obtained so far remains insufficient to unequivocally define the parts functionally important to the chromophore binding site.[30] The reason for this seems to be that the refinement software for X-ray structures does not include parameters for chemically unusual structures such as the twisted extended π-system of the retinyl chromophore or the carboxylate group of Glu-113 interacting with the delocalized charge in the chromophore.

In the absence of an unequivocal X-ray definition of the chromophore-binding site, the elucidation of the orientation and conformation of the pSB retinyl chromophore in rhodopsin continues to be the subject of much spectroscopic analysis, including rather heroic efforts in NMR spectroscopy[21,31−44] as well as FTIR[45−47] and resonance Raman spectroscopic studies.[48−51] While the experimental data reported in these studies have been reproduced and are considered unambiguous, the theoretical interpretation of the data does not yet lead to a fully consistent molecular picture in terms of the spatial, electronic, and vibrational structure of the system.[52]

The problem to be solved involves a challenging chromophore with a polarizable π-system embedded in a classical protein environment, an ideal system for applications of quantum mechanical/molecular mechanics (QM/MM) hybrid methods. QM/MM hybrid methods,[7−12] originally due to Warshel,[53] presently offer the most rigorous available methodologies to develop atomistic models from high-resolution X-ray structures and to investigate the electronic, vibrational, and nuclear magnetic resonance (NMR) properties of challenging chromophore prosthetic groups embedded in biological molecules.[54] This paper is focused on the application of DFT QM/MM hybrid methods, in an effort to provide rigorous interpretations of NMR experiments and fundamental insight on how the structure of the ligand-binding pocket determines the spectroscopic properties and functionality of the chromophore.

Many theoretical studies on rhodopsin were performed long before the high-resolution crystallographic X-ray structures were available.[25,55−72] The early studies by Warshel and co-workers[56−58] were focused on the analysis of the photoisomerization process in terms of the semiempirical QCFF/PI method for the description of the chromophore and a description of the protein environment based on a surface of closed-packed spheres with adjustable parameters. The QCFF/PI surfaces have been recalibrated[71] on the basis of ab initio studies of the isolated chromophore[66,67] and applied to studies of bacteriorhodopsin.[71] Further, the MNDO/AM1 and INDO-PSDCI procedures have been implemented by Birge and co-workers[59,61,64] to describe the photoisomerization dynamics in terms of a one-dimensional potential model with an arbitrary rate constant for the dissipation of internal energy. However, rigorous molecular models and simulations of NMR spectroscopy were not possible since the protein structure was not known.

The availability of high-resolution X-ray structures, combined with advances in the development of QM/MM hybrid methods,[7−12] offers a great opportunity to develop rigorous atomistic models. High-resolution X-ray structures have already motivated theoretical work focused on the analysis of the geometry and electronic excitation of the retinyl chromophore. The reported studies include calculations based on classical molecular dynamics simulations,[73−75] ab initio restricted Hartree−Fock (RHF) calculations of reduced-model systems,[76,52] and QM/MM computations.[16,30,77−80]

The ^{1}H and ^{13}C NMR spectra reported in this paper are based on the atomistic computational models of rhodopsin and bathorhodopsin developed in previous work,[16] in an effort to provide an explicit and rigorous description of the influence of the opsin environment on the ^{1}H and ^{13}C NMR chemical shifts of the retinyl chromophore. The models are able to predict the energy storage and electronic excitation energies for the dark and product states in very good agreement with experimental data.[16] However, there is the nontrivial question as to whether simulations of NMR spectroscopy, based on these computational models, are able to reproduce experimental data. This paper shows the affirmative, that such models predict NMR chemical shifts in very good agreement with solid-state NMR spectra of the retinyl chromophore in rhodopsin and bathorhodopsin. In addition to the obvious advance associated with validating prototypical GPCR models, these calculations show that QM/MM geometry optimization of high-resolution structural data provides a rigorous technique to overcome the limitations of traditional refinement methods and a general approach for simulating the spectroscopy of prosthetic groups embedded in biological molecules.

The paper is organized according to the following sections. Section 2 outlines the preparation of computational models of the 11-*cis*-retinyl chromophore in rhodopsin and in chloroform solution. Section 3 outlines the computational approach, including a description of the implementation of the ONIOM electronic-embedding hybrid method for computations of ^{1}H and ^{13}C NMR chemical shifts according to the GIAO acpproach. Section 4 presents the computational results organized in five subsections: Section 4.1 reports the computed ^{1}H NMR chemical shifts of rhodopsin and the comparison to solid-state NMR data. Section 4.1 also reports the computed ^{1}H NMR chemical shifts of the pSB 11-*cis*-retinyl chromophore in chloroform solution and the comparison to the corresponding experimental data. Section 4.2 discusses the conformation of the retinyl chromophore, with emphasis on the 6s-cis and 6s-trans configurations about the C6−C7 single bond. Section 4.3 reports ^{13}C NMR chemical

shifts of the 11-*cis*-retinyl chromophore in rhodopsin and in chloroform solution as well as the corresponding comparisons to experimental data. Section 4.4 compares the computed ^{13}C NMR chemical shifts of the *all-trans*-retinyl chromophore in bathorhodopsin with available solid-state NMR data. Finally, section 4.5 compares the rhodopsin computational model investigated in this paper to other structures of bovine visual rhodopsin available in the literature. Section 5 summarizes the computational findings and concludes.

2. Computational Models

Rhodopsin. A detailed description of the computational models and methods implemented in the present QM/MM study can be found in our recent work.[16] Here, we briefly summarize the underlying methodology as follows. The rhodopsin models are based on the refinement of the crystal structure of bovine rhodopsin (Protein Data Bank (PDB) accession code 1F88, monomer A), solved at 2.8 Å resolution.[26] Starting from the 1F88 PDB crystal structures, hydrogen atoms are added by using the molecular modeling program TINKER.[81] The protonation of all titratable groups is standard. The rhodopsin cavity is set neutral, consistently with FTIR experiments.[45] The pSB linkage between Lys-296 and the chromophore bears a net positive charge NH(+) that forms a salt-bridge with the Glu-113 negative counterion.[82,83] Amino acid residues Glu-122, Asp-83, and Glu-181, all within the protein core, are assumed to be neutral, as indicated by FTIR experiments[45] and UV−vis spectroscopic measurements of site-directed mutants.[84] Finally, the regular ends of the protein and the artificial ends due to the missing or incomplete amino acids from the X-ray structures in the third cytoplasmic loop (236−239) and in the C-terminal tail (328−348) are capped with NH_3^+ and CO_2^-. The complete model system in the present calculations contains 5170 atoms with a total charge of $+4e$.

Model systems based on the crystal structure with PDB accession code 1L9H, monomer A, solved at 2.6 Å resolution[29] have also been prepared. A crucial difference between the 1F88 and 1L9H crystal structures is the presence of two water molecules next to the retinyl chromophore in the 1L9H structure not observed at the lower resolution. These two water molecules are included in the computational model investigated in this paper, since they are important to the stabilization of the chromophore inside the protein cavity. Specifically, according to the computational models implemented in this paper, these two water molecules participate in an extended hydrogen-bonding network (see Figure 2), that involves both water molecules and polar residues Glu-181, Cys-187, Ser-186, and Glu-113.[16] This structural feature associated with the extracellular loop II (EII), folded next to the chromophore, is consistent with a recently proposed counterion switch mechanism associated with a subsequent step in the rhodopsin photobleaching sequence.[85,86]

The geometry of the resulting protein model is relaxed at the ONIOM-EE (B3LYP/6-31G*:Amber) level of theory by using Gaussian G03,[87] including the retinyl chromophore, bound water molecules, and all residues within a 20 Å radius from the chromophore. The remaining environment is subject to harmonic constraints in order to preserve the overall shape of the protein.

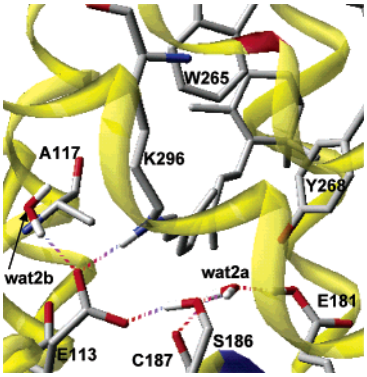

Figure 2. QM/MM optimized structure of the rhodopsin binding site, including the retinyl chromophore, the residues referenced in the text and the hydrogen bond network extending from E181 to E113.

The construction of the activated state is based on the assumption that the isomerization dynamics of the retinyl chromophore is much faster than protein relaxation. This assumption is consistent with the experimental 200 fs reaction time[21,22] as well as with the observation that the isomerization coordinate is mainly coupled to the vibrational modes of the retinyl chromophore.[50] It is also assumed that the molecular structure of the *all-trans*-retinyl chromophore in the ground-electronic state, produced by the underlying curve-crossing dynamics after photoexcitation of the system, *relaxes to the same minimum* energy configuration as when the chromophore is isomerized along the ground-state minimum energy path (MEP) subject to the constraint of fixed protein environment.[16] These assumptions are consistent with the recent observation of thermal activation of visual pigments,[88] indicating that activation by light and by heat may in fact follow the same molecular route.

The reactant and product minimum energy configurations are subsequently used for generating an ensemble of thermally accessible configurations according to importance sampling Monte Carlo, with umbrella sampling functions defined in terms of the DFT QM/MM minimum energy configurations. An ensemble of 1000 thermal configurations are generated at 300 K from a Markov chain of 900 000 configurations generated by importance sampling Monte Carlo, using Boltzmann sampling functions defined by the classical energy (e.g., the standard Amber-MM force field with additional soft-harmonic constraints relative to the QM/MM equilibrium geometries). The statistical factors (weights) of the subset of 1000 importance sampled configurations are subsequently reweighted by performing single point calculations at the ONIOM-EE(B3LYP/6-31G*:Amber) level and computing the corresponding Boltzmann factors defined by the difference of ONIOM-EE (B3LYP/6-31G*:Amber) and classical energies. The equilibrium geometry as well as the thermal fluctuations for the 11-cis conformation at 300 K compare very favorably to recently reported results of Molecular Dynamics (MD) simulations at the QM/MM(SCC-DFTB:CHARMM) level of theory,

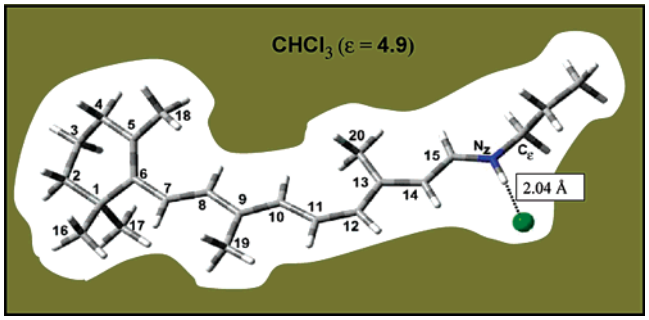

Figure 3. Optimized structure of the 11-*cis*-retinyl propylinium chloride complex embedded in a PCM solvent with $\epsilon = 4.9$ (chloroform).

where in agreement with our work, all simulated annealing minimizations converged to the same minimum energy structure.[30] Considering the usual symmetry of magnetic shielding matrix elements, relative to fluctuations around equilibrium configurations, it is therefore natural to expect that such a minimum energy configuration provides the dominant contribution to thermal ensemble averages.

pSB Model. To compare changes in the NMR spectroscopy of the retinyl chromophore inside the protein, relative to the corresponding spectrum of the chromophore in solution,[31] computational models of the 11-*cis*-retinyl propylinium−chloride complex in chloroform solution are constructed by geometry optimization at the DFT B3LYP/6-31G* level of theory of the complex embedded in a polarizable continuum model (PCM) solvent ($\epsilon_{sol} = 4.9$). Figure 3 shows the optimized configuration of the complex, where the chloride ion is located in the C=NH+plane at 2.09 Å from the proton of the Schiff-base linkage.

3. Methods

The QM/MM(MO:MM) calculations reported in this paper are based on the ONIOM two-layer hydrogen link-atom scheme.[7−13] The full system of 5170 atoms is partitioned into two layers by imposing a frontier, between the QM and MM layers, at the $C_\delta-C_\epsilon$ bond of the Lys-296 side chain (i.e., two bonds beyond the C−NH(+) linkage). The quantum mechanical (QM) layer includes 48 atoms of the retinyl chromophore, five atoms of Lys-296 (NH^+, CH_2), and a link hydrogen atom that saturates the extra valence of the terminal $-C-H_2$ at the boundary. While a QM layer that includes only the retinyl chromophore is sufficient to describe the optimum geometry of the system as well as conformational changes due to 11-cis/all-trans isomerization, the analysis of numerical convergence with respect to the size of the QM layer indicates that precise calculations of ^{1}H and ^{13}C NMR chemical shifts require a more extended QM layer. Thus single point calculations of chemical shifts explicitly consider extended QM layers including amino acid residues with significant steric interactions with the chromophore as well as nearby residues with aromatic functional groups, including Trp-265, Tyr-268, Ser-186, Cys-187, and Gly-188. Inclusion of these extra residues results in a QM layer with 80 additional atoms, including the six link-hydrogen atoms placed at the C−N bonds connecting these five residues with their neighbors. The remainder of the protein defines the MM layer.

The total energy of the system E is obtained according to the *ONIOM electronic-embedding* (ONIOM-EE) approach

$$E = E^{MM,full} + E^{QM,red} - E^{MM,red} \quad (1)$$

where $E^{MM,full}$ is the energy of the full system computed at the MM level of theory, $E^{QM,red}$ is the energy of the reduced system computed at the QM level of theory, and $E^{MM,red}$ is the energy of the reduced system computed at the MM level of theory. Electrostatic interactions between the two layers are included in the calculation of both $E^{QM,red}$ and $E^{MM,red}$ at the QM and MM levels, respectively. Therefore, the electrostatic interactions included at the MM level in both terms $E^{MM,red}$ and $E^{MM,full}$ cancel. The resulting QM description includes polarization of the reduced system as induced by the surrounding protein environment.

All calculations reported in this paper involve a description of the MM layer modeled by the standard Amber force field.[89] Shielding constants (i.e., chemical shifts) are obtained according to the GIAO method at the DFT ONIOM-EE (B3LYP/6-31G*:Amber) level of theory. The ability of the B3LYP hybrid density functional to reproduce experimental NMR shielding constants with similar basis sets is well documented.[90] Details concerning the calculation of shielding constants are not discussed in this paper since they have already been extensively reviewed in the literature.[91] However, it is important to mention that in order to facilitate the comparison between theoretical and experimental values of shielding constants, often reported relative to various different internal or external references, ab initio chemical shifts are reported relative to the reference value that minimizes the overall root-mean-squared deviation between the ab initio and experimental NMR spectra. All chemical shifts are expressed as usual in parts per million (ppm). Therefore, a chemical shift at δ ppm indicates that the nucleus responsible for the signal is magnetically unshielded relative to the reference and requires a magnetic field δ millionths less than the field needed by the reference to produce resonance.

4. Results and Discussion

4.1. Rhodopsin ^{1}H NMR. Figure 4 and Table 1 (columns 2 and 3) compare the calculated ^{1}H NMR chemical shifts of the 11-*cis*-retinyl chromophore in rhodopsin and the chemical shifts of the 11-*cis*- retinyl propylinium−chloride complex in chloroform solution to the corresponding values of experimental data. The agreement between ab initio and experimental values indicates that the computational models are able to reproduce the ^{1}H NMR spectroscopy of the chromophore in both the rhodopsin and solution environments, including the significant differences in chemical shifts between the more unshielded H atoms attached to sp^2 carbon atoms in the C7−C15 segment ($\sigma^P = 6-7$ ppm range) and the more protected sp^3 carbon atoms ($\sigma^C = 0.3-2$ ppm range) in the methyl substituent groups and the β-ionone ring.

Figure 5 and Table 1 (column 4) present the theoretical and experimental values of *changes* in the chromophore ^{1}H NMR chemical shifts, $\Delta\sigma^H = \sigma^H_{rhod} - \sigma^H_{sol}$, due to the influence of the rhodopsin environment (i.e., the opsin effects

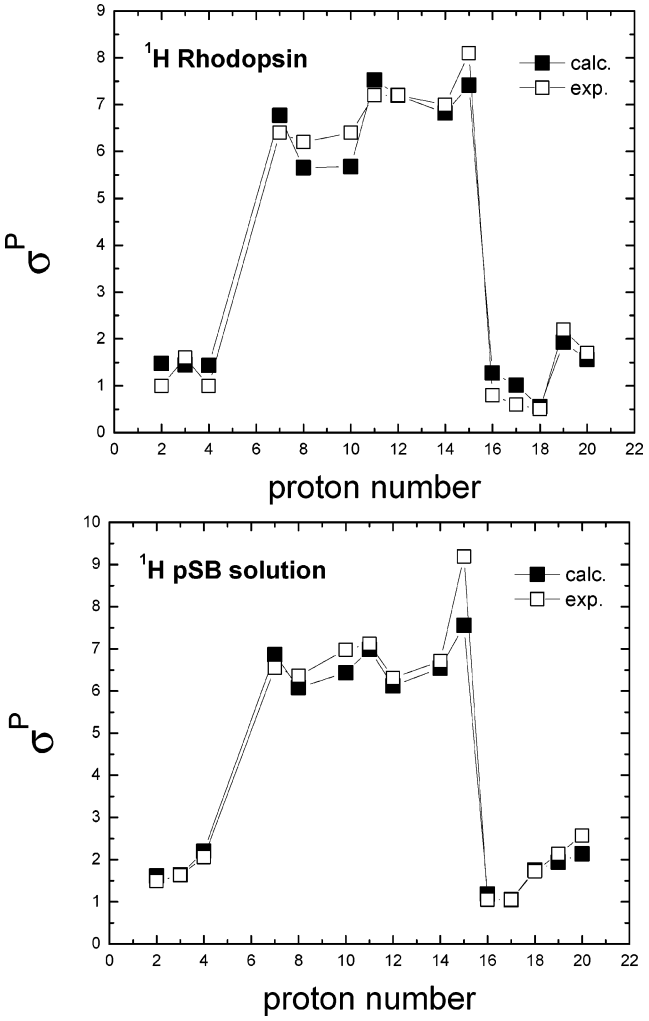

Figure 4. Comparison of ^{1}H NMR chemical shifts (in ppm) of the 11-*cis*-retinyl chromophore in rhodopsin σ^H_{rhod} (upper panel) and 11-*cis*-retinyl propylinium chloride complex in chloroform σ^H_{sol} (lower panel). H atoms are labeled as indicated in Figure 3.

on ^{1}H NMR chemical shifts). In semiquantitative agreement with the experimental data, the ab initio calculations predict that the most significant influence of the protein environment is to unshield H atoms in the C11−C14 segment, while nearby residues partially shield protons in the β-ionone ring, including H-4 and H-18. The theoretical predictions, however, underestimate changes in chemical shifts of H-15 and H-20 probably due to the oversimplified description provided by the reaction field of the PCM dielectric solvent, as indicated by the numerical deviations in Table 1 (column 3).

4.2. C6−C7 Bond Conformation. The configuration about the C6−C7 single bond of the 11-*cis* retinyl chromophore defines the orientation of the β-ionone ring relative to the polyene chain and has been the subject of debate in the literature.[32,40,42,72,92] In particular, NMR studies by Watts and co-workers[40] as well as theoretical work by Birge and co-workers[72] concluded that the chromophore geometry is 6s-trans at the C6−C7 bond, in contrast to the 6s-cis conformation assumed by earlier NMR and optical studies.[32,42,93−96] It is therefore of interest to analyze this

Table 1: Comparison of ^{1}H NMR Chemical Shifts (in ppm) of the 11-*cis*-Retinyl Chromophore in Rhodopsin σ^H_{rhod}, the 11-*cis*-Retinyl Propylinium−Chloride Complex in Chloroform Solution σ^H_{sol}, and Opsin Effects on ^{1}H NMR Chemical Shifts as Defined by $\Delta\sigma^H = \sigma^H_{rhod} - \sigma^H_{sol}$[a]

position	σ^H_{rhod}	σ^H_{sol}	$\Delta\sigma^H$
H-2	1.18 (1.0)[b]	1.61 (1.49)[c]	−0.43 (−0.49)
H-3	1.00 (1.6)[b]	1.64 (1.63)[c]	−0.64 (−0.03)
H-4	0.97 (1.0)[b]	2.20 (2.06)[c]	−1.23 (−1.06)
H-7	6.81 (6.4)[b]	6.86 (6.55)[d]	−0.05 (−0.15)
H-8	6.11 (6.2)[b]	6.09 (6.36)[d]	0.02 (−0.16)
H-10	6.19 (6.4)[b]	6.44 (6.98)[d]	−0.25 (−0.58)
H-11	7.62 (7.2)[b]	6.99 (7.12)[d]	0.63 (0.08)
H-12	7.26 (7.2)[b]	6.13 (6.31)[d]	0.13 (0.89)
H-14	6.85 (7.0)[b]	6.54 (6.71)[d]	0.31 (0.29)
H-15	7.35 (8.1)[b]	7.55 (9.19)[d]	−0.20 (−1.09)
H-16	0.89 (0.8)[b]	1.18 (1.05)[d]	−0.29 (−0.25)
H-17	0.84 (0.6)[b]	1.05 (1.05)[d]	−0.21 (−0.45)
H-18	0.28 (0.5)[b]	1.76 (1.73)[d]	−1.48 (−1.23)
H-19	2.05 (2.2)[b]	1.94 (2.14)[d]	0.11 (0.06)
H-20	1.98 (1.7)[b]	2.14 (2.57)[d]	−0.16 (−0.87)

[a] Experimental values are reported between parentheses. H atoms are labeled as indicated in Figure 3. [b] Data from ref 42. [c] Data from ref 99. [d] Data from ref 31.

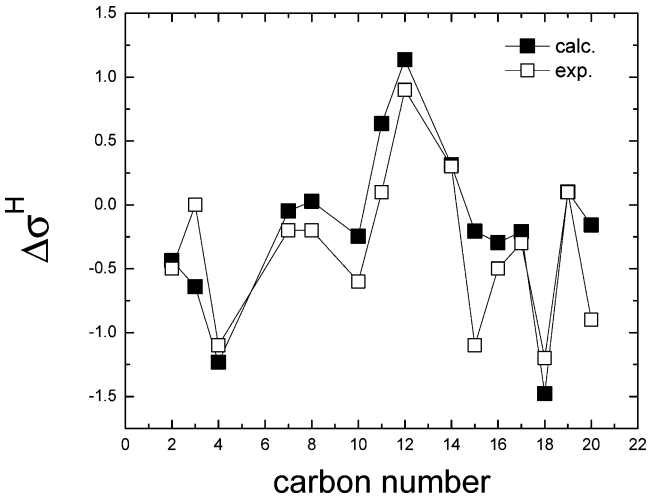

Figure 5. Comparison of theoretical and experimental values of *changes* in the ^{1}H NMR chemical shifts of the 11-*cis*-retinyl chromophore (in ppm), $\Delta\sigma^H = \sigma^H_{rhod} - \sigma^H_{sol}$, due to the influence of the rhodopsin environment (i.e., the opsin effects on ^{1}H NMR chemical shifts as described in the text).

controversial aspect by simulating the ^{1}H NMR spectra for the retinyl chromophore in rhodopsin for both the 6s-cis and 6s-trans conformations and comparing these theoretical predictions to the ^{1}H NMR experimental spectrum.

To perform these calculations, a computational model of the 6s-trans isomer was constructed by geometry relaxation of the system after rotation of the β-ionone ring around the C6−C7 bond. The resulting 6s-trans structure, obtained at the ONIOM electronic-embedding (B3LYP/6-31G*:Amber) level of theory, was found to be as stable as the 6s-cis isomer for most thermally accessible configurations and about 8 kcal/mol less stable than the 6s-cis structure when comparing minimum energy geometries. In addition, the ^{1}H NMR spectrum of the 6s-trans isomer compares much less favor-

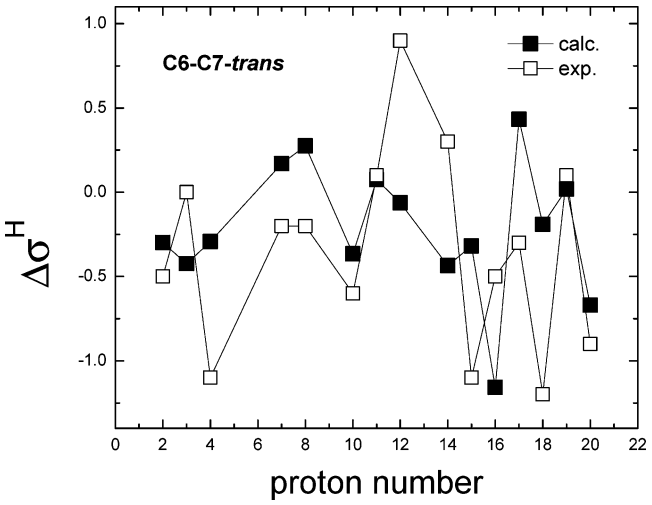

Figure 6. Changes in the ^{1}H NMR chemical shifts of the 6*s-trans*-retinyl chromophore, $\Delta\sigma^H = \sigma^H_{rhod} - \sigma^H_{sol}$, due to the influence of the rhodopsin environment. Theoretical values are compared to experimental data.

ably to experiments than the spectrum of the 6s-cis isomer, as shown in Figures 6 and 5. Figure 6 compares the opsin effects on the ^{1}H NMR chemical shifts of the 6s-trans chromophore ($\Delta\sigma^H = \sigma^H_{rhod} - \sigma^H_{sol}$) to experimental data, indicating that the 6s-trans isomer compares less favorably to experiments than the 6s-cis isomer analyzed in Figure 5.

The comparison of theoretical and experimental ^{1}H NMR chemical shifts presented in Figures 6 and 5, in conjunction with the analysis of relative stabilities, indicates that the orientation of the β-ionone ring relative to the polyene chain is consistent with the 6s-cis configuration of the retinyl chromophore at the C6−C7 single bond. The QM/MM computational models reported in this paper thus support the 6s-cis form, with substantial negative (−44°) twist of the C6−C7 bond in the minimum energy configuration.[16] These computational results are partially consistent with recent NMR studies[42,92] and with the analysis of the recently resolved X-ray structure at 2.2 Å resolution.[30]

4.3. Rhodopsin ^{13}C NMR. Figure 7 and Table 2 (columns 2 and 3) compare theoretical and experimental values of ^{13}C NMR chemical shifts of the 11-*cis*-retinyl chromophore in rhodopsin as well as the corresponding chemical shifts of the 11-*cis*-retinyl propylinium−chloride complex in chloroform solution. The agreement, shown in Figure 7, indicates that the computational models are able to reproduce the ^{13}C NMR spectroscopy of the chromophore in both rhodopsin and solution environments, including the description of significant differences in chemical shifts between the unshielded carbon atoms with sp^2 hybridization in the C7−C15 segment (σ^C = 115−160 ppm range) and the more protected sp^3 carbon atoms (σ^C = 20−40 ppm range).

A common feature of the ^{13}C NMR spectra of the pSB in rhodopsin (Figure 7, upper panel) and in solution (Figure 7, lower panel) is the zigzag alternation of chemical shifts in the C9−C15 segment of the polyene chain, where the displacement maxima at C15, C13, C11, and C9 are alternated with the minima at C14, C12, and C10. Such an alternation pattern is partially correlated with a corresponding

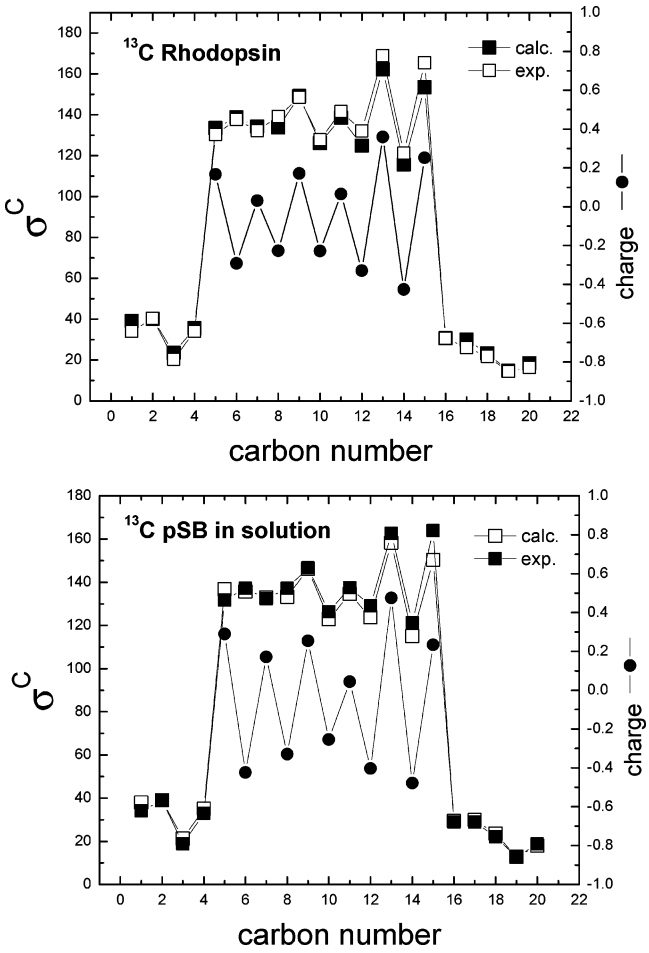

Figure 7. Comparison of ^{13}C NMR chemical shifts (in ppm) of the 11-*cis*-retinyl chromophore in rhodopsin σ^C_{rhod} (upper panel) and the 11-*cis*-retinyl propylinium−chloride complex in chloroform σ^C_{sol} (lower panel). ESP atomic charges of carbon atoms with sp^2 hybridization are reported in solid circles.

alternation of the atomic charges of carbon atoms with sp^2 hybridization along the polyene chain (see solid circles in Figure 7).

Figure 8 and Table 2 (column 4) compare theoretical and experimental values of *changes* in the chromophore ^{13}C NMR chemical shifts, $\Delta\sigma^C = \sigma^C_{rhod} - \sigma^C_{sol}$, due to the influence of the rhodopsin environment (i.e., the opsin effects on ^{13}C NMR chemical shifts). Considering that the reported experimental errors of ^{13}C NMR chemical shifts can be as large as ±1 ppm,[32,42] and larger when comparing different studies, the overall semiquantitative agreement with experimental data is quite satisfactory. The theoretical predictions, however, seem to underestimate changes in chemical shifts of C17 and C20. This is due to an overestimation of the chemical shifts of the corresponding methyl substituent groups in rhodopsin, as indicated by the numerical deviations in Table 2 (column 2). In agreement with experimental data, these results predict that the protein environment unshields all C atoms but C5 in the retinyl chromophore polyene chain.

The upfield of σ^C at C5 has been assigned to the interaction between C5 and the carboxylic group of Glu-122.[42] The calculations reported in this paper, however, indicate that the electrostatic influence of Glu-122 is negligible when such

Table 2: Comparison of ^{13}C NMR Chemical Shifts (in ppm) of the 11-*cis*-Retinyl Chromophore in Rhodopsin σ^{C}_{rhod}, the 11-*cis*-Retinyl Propylinium−Chloride Complex in Chloroform Solution σ^{C}_{sol}, and Opsin Effects on ^{13}C NMR Chemical Shifts as Defined by $\Delta\sigma^{C} = \sigma^{C}_{rhod} - \sigma^{C}_{sol}$[a]

position	σ^{C}_{rhod}	σ^{C}_{sol}	$\Delta\sigma^{C}$
C1	39.06 (34.0)[b]	37.97 (34.1)[b]	1.09 (−0.1)
C2	40.08 (40.3)[b]	39.03 (38.9)[b]	1.05 (1.4)
C3	23.45 (20.3)[b]	21.23 (18.8)[b]	2.22 (1.5)
C4	35.52 (34.0)[b]	35.13 (33.0)[b]	0.39 (1.0)
C5	133.43 (130.3)[c]	136.66 (131.7)[d]	−3.23 (−1.4)
C6	138.77 (137.7)[c]	135.69 (137.2)[d]	3.08 (0.5)
C7	134.21 (132.3)[c]	132.89 (132.3)[d]	1.32 (0.0)
C8	133.78 (139.2)[c]	133.27 (137.2)[d]	0.51 (2.0)
C9	149.09 (148.5)[c]	146.20 (146.6)[d]	2.89 (1.9)
C10	126.11 (127.8)[c]	122.94 (126.4)[d]	3.17 (1.4)
C11	138.55 (141.6)[c]	134.61 (137.5)[d]	3.94 (4.1)
C12	124.89 (132.1)[c]	123.70 (129.0)[d]	1.19 (3.1)
C13	162.18 (168.9)[c]	158.28 (162.7)[d]	3.90 (6.2)
C14	115.60 (121.2)[c]	115.04 (121.3)[d]	0.56 (−0.1)
C15	153.49 (165.4)[c]	150.31 (163.9)[d]	3.18 (1.5)
C16	30.60 (30.6)[b]	29.47 (28.9)[b]	1.13 (1.7)
C17	29.96 (26.1)[b]	29.91 (28.9)[b]	0.05 (−2.8)
C18	23.28 (21.7)[b]	23.54 (22.1)[b]	−0.26 (−0.4)
C19	14.73 (14.4)[b]	12.81 (12.6)[b]	1.92 (1.8)
C20	18.42 (16.3)[b]	17.88 (18.8)[b]	0.54 (−2.5)

[a] Experimental values are reported between parentheses. [b] Data from ref 42. [c] Data from ref 32. [d] Data from ref 31.

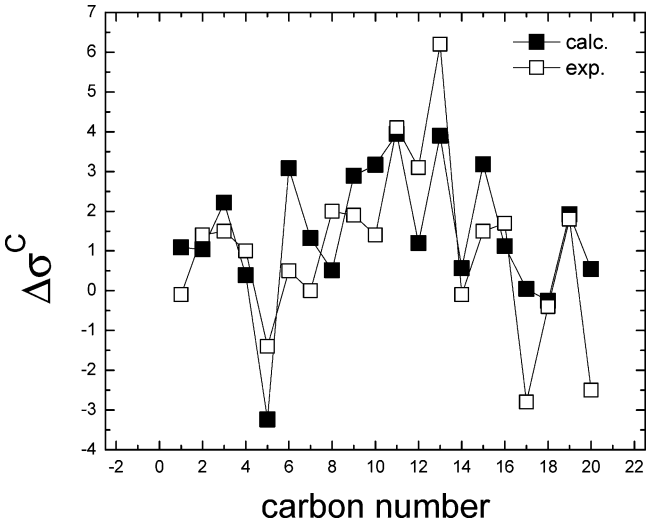

Figure 8. Comparison of theoretical and experimental values of *changes* in the ^{13}C NMR chemical shifts of the 11-*cis*-retinyl chromophore (in ppm), $\Delta\sigma^{H} = \sigma^{C}_{rhod} - \sigma^{C}_{sol}$, due to the influence of the rhodopsin environment (i.e., the opsin effects on ^{13}C NMR chemical shifts).

a residue is protonated as suggested by FTIR experiments.[45] Instead, Table 3 shows that the most important upfield effect on C5 is due to Trp-265, with an upfield of −2.0 ppm. This effect, however, is almost completely canceled by the 1.8 ppm downfield due to Asp-190. It is, therefore, concluded that the net upfield of σ^{C} at C5 is not determined by the nearby residue with the largest upfield contribution but rather by the overall polarization of the π-system, predominantly modulated by the counterion Glu-113. Further, it is predicted

Table 3: List of Residues with Significant Contribution on the Opsin Shift, $\Delta\sigma^{C}$[a]

	upfield		downfield	
position	residue	$\Delta\sigma^{C}$ (ppm)	residue	$\Delta\sigma^{C}$ (ppm)
C1	Glu-122	−0.2	His-211	0.1
C2	Asp-190	−0.1	Phe-212	0.6
C3	Tyr-268	−0.2	Glu-122	0.2
C4	Leu-125	−0.2	Glu-122	0.3
C5	Trp-265	−2.0	Asp-190	1.8
C6	Glu-201	−1.0	Trp-265	0.9
C7	Tyr-191	−1.6	Cys-187	1.7
C8	Asp-190	−0.3	Trp-265	0.5
C9	Thr-118	−2.3	Cys-187	2.2
C10	Tyr-268	−1.2	Tyr-191	1.2
C11	Thr-118	−1.8	Gly-188	2.2
C12	Cys-187	−2.2	Ala-117	1.7
C13	Wat2a	−2.7	Tyr-191	0.6
C14	Cys-187	−3.0	Wat2a	3.0
C15	Ala-292	−1.6	Glu-181	0.5
C16	His-211	−0.1	Met-207	0.5
C17	Tyr-268	−0.4	Tyr-191	0.3
C18	Thr-118	−0.2	Gly-121	1.3
C19	Thr-118	−0.9	Glu-122	0.1
C20	Wat2a	−0.5	Tyr-268	0.3

[a] This table quantifies the effect on the ^{13}C NMR chemical shifts as described in the text.

that mutations of either Trp-265 or Asp-190 are expected to produce a significant effect on the ^{13}C NMR spectrum at the C5 position.

For completeness, Table 3 presents the quantitative analysis of the electrostatic influence of nearby amino acid residues on the ^{13}C NMR chemical shifts of the retinyl chromophore. Individual contributions are estimated as the difference in chemical shifts after and before zeroing the atomic charges of specific residues. For clarity, only the residues with the largest upfield and downfield effects are listed. Table 3 thus identifies the specific residues responsible for producing the most significant influence, indicating that nearby residues can cause $\Delta\sigma^{C}$ values as large as ±3 ppm for carbon atoms in the conjugate π-system (i.e., carbon atoms with sp^2 hybridization). In contrast, chemical shifts of carbon atoms with sp^3 hybridization (e.g., carbon atoms in methyl substituent groups) are found to be significantly less sensitive to the electrostatic influence of nearby polar residues (e.g., $|\Delta\sigma^{C}| < 1$ ppm).

4.4. Bathorhodopsin ^{13}C NMR. Figure 9 (upper panel) and Table 4 (second column) compare the calculated ^{13}C NMR chemical shifts of the *all-trans*-retinyl chromophore in bathorhodopsin to readily available experimental data, including ^{13}C NMR chemical shifts for C8, C10, C11, C12, C13, C14, and C15.[33] In addition, Table 4 (third column) and Figure 9 (lower panel) present theoretical and experimental values of *changes* in the chromophore ^{13}C NMR chemical shifts, $\Delta\sigma^{C} = \sigma^{C}_{batho} - \sigma^{C}_{rhod}$, due to the 11-cis/all-trans isomerization. The comparison presented in Figure 9 shows good qualitative agreement between theoretical and existing experimental data, supporting the underlying molecular rearrangements due to the primary photochemical event reported in previous work.[16]

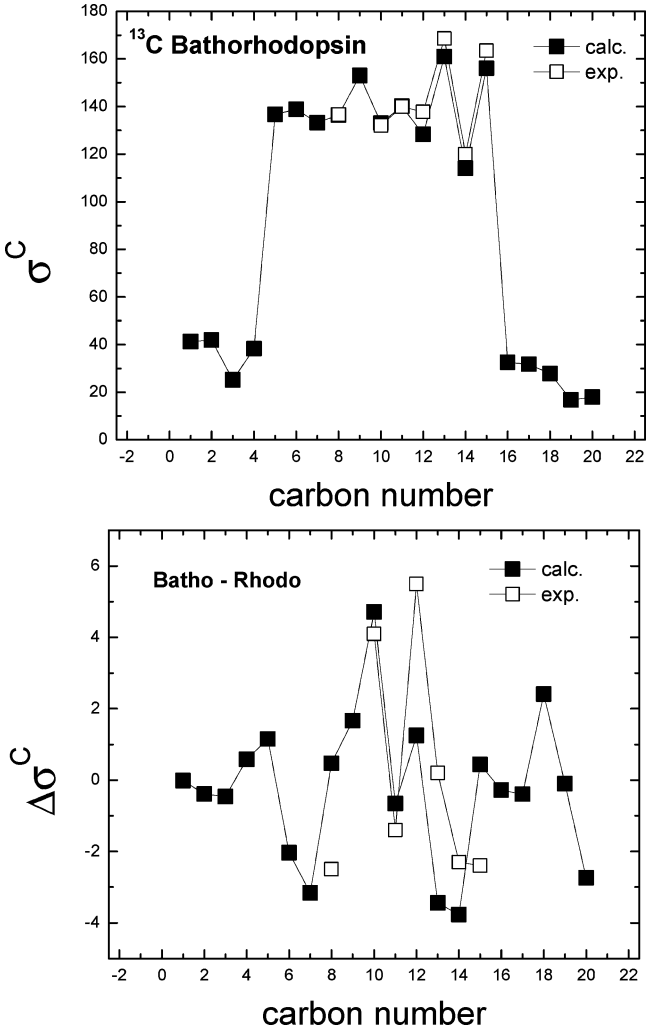

Figure 9. Comparison of ^{13}C NMR chemical shifts (in ppm) of the *all-trans*-retinyl chromophore in bathorhodopsin σ^{C}_{rhod} (upper panel) and the difference between ^{13}C NMR chemical shifts in bathorhodopsin and rhodopsin (lower panel).

The favorable comparison of theoretical and experimental values of changes in ^{13}C NMR chemical shifts, due to the cis/trans isomerization, is consistent with the agreement between theoretical and experimental values of other observables determined by the molecular rearrangements, including the endothermicity of the cis/trans isomerization as compared to calorimetry measurements and the $S_0 \rightarrow S_1$ electronic excitation energies for the dark and product states as compared to readily available spectroscopic data. It is therefore concluded that the ϕ(C11−C12) dihedral angle changes from −11° in the 11-cis isomer to −161° in the all-trans product during the primary event, as predicted in previous work,[16] where the preferential sense of rotation along negative angles is determined by steric interactions between Ala-117 and the polyene chain at the C13 position. The isomerization also induces torsion of the polyene chain due to other steric constraints in the binding pocket and stretching of the salt-bridge between the protonated Schiff-base and the Glu-113 counterion. The salt-bridge stretching is stabilized by the formation of a hydrogen bond between the protonated Schiff-base and Wat2b,[16] involving reorientation of the polarized NH+ and CH bonds localizing part of the net positive charge at the Schiff-base linkage.

Table 4: Comparison of ^{13}C NMR Chemical Shifts (in ppm) of the *all-trans*-Retinyl Chromophore in Bathorhodopsin σ^{C}_{batho} and *Changes* in the Chromophore ^{13}C NMR Chemical Shifts, $\Delta\sigma^{C} = \sigma^{C}_{batho} - \sigma^{C}_{rhod}$, Due to the 11-Cis/All-Trans Isomerization[a]

position	σ^{C}_{batho}	$\Delta\sigma^{C}$
C1	39.05	−0.01
C2	39.69	−0.39
C3	22.98	−0.46
C4	36.10	0.58
C5	134.58	1.15
C6	136.73	−2.04
C7	131.05	−3.17
C8	134.25 (136.6)[b]	0.47 (−2.5)[c]
C9	150.76	1.67
C10	130.82 (132.0)[b]	4.71 (4.1)[c]
C11	137.90 (140.0)[b]	−0.65 (−1.4)[c]
C12	126.14 (137.7)[b]	1.25 (5.5)[c]
C13	158.74 (168.5)[b]	−3.44 (0.2)[c]
C14	111.83 (120.0)[b]	−3.77 (−2.3)[c]
C15	153.92 (163.4)[b]	0.43 (−2.4)[c]
C16	30.32	−0.28
C17	29.56	−0.40
C18	25.69	2.41
C19	14.63	−0.10
C20	15.68	−2.74

[a] Experimental values are reported between parentheses. [b] Data from ref 33. [c] Data from ref 32.

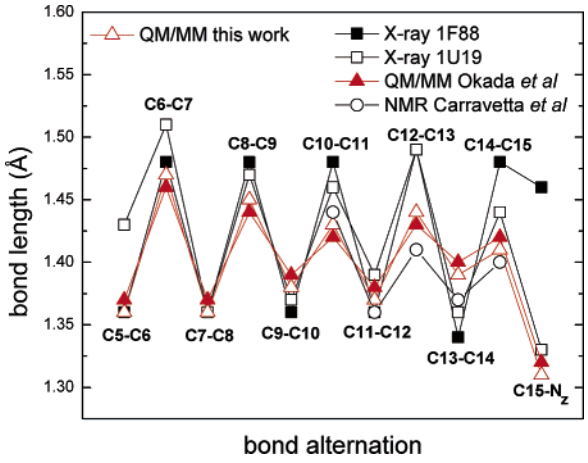

Figure 10. Bond length alternation along the polyene chain of the 11-*cis*-retinyl chromophore in rhodopsin.

4.5. Comparative Structural Analysis. After the computational studies reported in the previous sections were completed, the latest refinement of the rhodopsin crystal structure was published at 2.2 Å resolution,[30] together with a QM/MM structural analysis based on the self-consistent charge density functional tight binding (SCC-DFTB) method[97] and the CHARMM force field.[98] Therefore, it is of interest to compare the structural properties of the rhodopsin computational model analyzed in this paper to the more recently published molecular structures.

Figure 10 and Table 5 compare the chromophore bond lengths in readily available X-ray structures and QM/MM

Table 5: Comparison of the Retinyl Chromophore Bond Lengths in Readily Available X-ray Structures and QM/MM Computational Models, Including the Crystal Structures with PDB Access Code 1F88,[26] 1HZX,[28] 1L9H,[29] and 1U19,[30] the QM/MM-MD (SCC-DFTB:CHARMM) Structure,[30] and the QM/MM ONIOM-EE (B3LYP:Amber) Structure Analyzed in This Paper and in Previous Work[16]

	1F88	1HZX	1L9H	1U19	QM/MM[a]	QM/MM[b]	NMR[c]
C5−C6	1.36	1.36	1.41	1.43	1.37	1.36	
C6−C7	1.48	1.51	1.50	1.51	1.46	1.47	
C7−C8	1.36	1.38	1.37	1.36	1.37	1.36	
C8−C9	1.48	1.49	1.47	1.47	1.44	1.45	
C9−C10	1.36	1.36	1.35	1.37	1.39	1.38	
C10−C11	1.48	1.48	1.49	1.46	1.42	1.43	1.44
C11−C12	1.36	1.37	1.37	1.39	1.38	1.37	1.36
C12−C13	1.49	1.50	1.48	1.49	1.43	1.44	1.41
C13−C14	1.34	1.36	1.36	1.36	1.40	1.39	1.37
C14−C15	1.48	1.50	1.51	1.44	1.42	1.41	1.43
C15−N(Lys-296)	1.46	1.36	1.36	1.33	1.32	1.31	
N(Lys-296)−O(Glu-113)	3.28	3.58	3.08	3.36	2.60	2.74	

[a] Reference 30. [b] This work and ref 16. [c] Reference 43.

computational models, including the 1F88, 1HZX, 1L9H, and 1U19 X-ray structures, the QM/MM-MD (SCC-DFTB:CHARMM) structure,[30] and the QM/MM ONIOM-EE (B3LYP:Amber) rhodopsin model[16] considered in this paper. The comparison includes bond lengths along the polyene chain and the salt-bridge between the protonated Schiff-base and the negative counterion Glu-113. All distances but those in the last two columns are averaged over both monomers. The comparison shows that the rhodopsin computational model investigated in this work is consistent with the QM/MM-MD (SCC-DFTB:CHARMM) structure.[30] However, when QM/MM models are compared to X-ray structures, both computational models show a weaker alternation of CC bond lengths along the polyene chain (see zigzag of red triangles in Figure 10), although in partial agreement with the chromophore bond lengths predicted by a recent double-quantum solid-state NMR study (see last column of Table 5 and open circles in Figure 10).[43] Furthermore, both QM/MM models predict a shorter N(Lys-296)−O(Glu-113) distance between the Schiff-base linkage and the counterion Glu-113.

The structural differences between X-ray and QM/MM structures seem to result from difficulties faced by the X-ray refinement software when dealing with chemically unusual structures, including the twisted and extended π-system and the carboxylate group interacting with the delocalized charge of the extended chromophore. Further, the X-ray structures show significant dispersion in the reported values of bond lengths and C11−C12 dihedral angles. The latter ranges from −36° in the 1U19 crystal structure,[30] to −1° in 1F88, 8° in 1HZX, and 0° in 1L9H. In contrast, the ONIOM-EE and SCC-DFTB QM/MM models have a smaller dispersion and predict the C11−C12 dihedral angle to be −11°[16] and −18° ± 9,[30] respectively, in reasonable agreement with the value −13° suggested by molecular dynamics simulations.[74]

An important difference between the QM/MM-MD (SCC-DFTB:CHARMM) structure[30] and the QM/MM ONIOM-EE (B3LYP:Amber) rhodopsin model analyzed in this paper[16] concerns the assignment of interactions responsible for twisting the extended π-system. Okada et. al. suggested, from simple inspection of neighboring residues, that the C11−C12 negative twist is due to interactions with the Trp-265 residue.[30] In contrast, the QM/MM ONIOM-EE model predicts that the torque responsible for the C11−C12 dihedral twist is mainly due to steric interactions between the methyl group of Ala-117 and the polyene chain at the C13 position.[16] These results are obtained from an analysis of the decomposition of forces acting on the chromophore at its equilibrium configuration in the binding site.

5. Concluding Remarks

We have shown how to investigate the ^{1}H NMR and ^{13}C NMR spectra of the retinyl chromophore in rhodopsin by using recently developed QM/MM computational models, in conjunction with the GIAO method for ab initio SCF calculations of NMR chemical shifts at the DFT (B3LYP/6-31G*:Amber) level of theory. The reported results indicate that the QM/MM models describe the NMR spectroscopy of the retinyl chromophore in rhodopsin in very good agreement with solid-state NMR experiments, including opsin effects on NMR chemical shifts and *changes* in the chromophore chemical shifts due to 11-cis/all-trans isomerization in rhodopsin. These findings are particularly relevant to the development and validation of fully atomistic models of prototypical G-protein-coupled receptors.

We have demonstrated that the 6s-cis/6s-trans configurational change, about the C6−C7 single bond of the 11-cis retinyl chromophore, significantly affects the ^{1}H NMR chemical shifts of the chromophore. The comparison of theoretical and experimental ^{1}H NMR spectra indicates that the 6s-cis isomer is the most likely structure in the dark state of rhodopsin. This conclusion is consistent with the analysis of relative stabilities, indicating that the 6s-cis configuration is 8 kcal/mol more stable than the 6s-trans configuration when comparing minimum energy structures.

We have shown that the QM/MM computational models reveal significant bond length alternation in the C5−C9 segment of the polyene chain. Such a bond length alternation pattern becomes weaker along the π-system near the Schiff-base linkage, in partial agreement with the chromophore bond lengths predicted by double-quantum solid-state NMR experiments.[43]

We found that ^{1}H NMR chemical shifts are considerably more sensitive than ^{13}C NMR chemical shifts to changes in the chromophore environment (e.g., from solution to the protein environment). In particular, the ^{1}H NMR spectra is found to be significantly influenced by nearby polar residues and residues with aromatic functional groups (e.g., Trp-265 and Tyr-268). Reliable QM/MM simulations of NMR chemical shifts thus require including these crucial residues in the QM layer, predicting specific phenotypes that affect the magnetic environment of the retinyl chromophore in rhodopsin.

Finally, we conclude that the QM/MM refinement of high-resolution structural data provides a rigorous technique to overcome limitations of traditional X-ray refinement methods

and a general approach to simulate the NMR spectroscopy of challenging prosthetic groups embedded in biological molecules.

Acknowledgment. V.S.B. acknowledges supercomputer time from the National Energy Research Scientific Computing (NERSC) Center and financial support from Research Corporation, Research Innovation Award # RI0702, a Petroleum Research Fund Award from the American Chemical Society PRF # 37789-G6, a junior faculty award from the F. Warren Hellman Family, the National Science Foundation (NSF) Career Program Award CHE # 0345984, the NSF Nanoscale Exploratory Research (NER) Award ECS # 0404191, the Alfred P. Sloan Fellowship from the Sloan Foundation, and start-up package funds from the Provost's office at Yale University. The authors are grateful to Mr. Sabas Abuabara for proofreading the manuscript.

References

(1) Ji, T.; Grossmann, M.; Ji, I. *J. Biol. Chem.* **1998**, *273*, 17299−17302.

(2) Gether, U.; Kobilka, B. *J. Biol. Chem.* **1998**, *273*, 17979−17982.

(3) Marinissen, M.; Gutkind, J. *Trends. Pharmacol. Sci.* **2001**, *22*, 368−376.

(4) Meng, E.; Bourne, H. *Trends. Pharmacol. Sci.* **2001**, *22*, 587−593.

(5) Baldwin, J.; Schertler, G.; Unger, V. *J. Mol. Biol.* **1997**, *272*, 144−164.

(6) Hamm, H. *Proc. Natl. Acad. Sci. U.S.A.* **2001**, *98*, 4819−4821.

(7) Maseras, M.; Morokuma, K. *J. Comput. Chem.* **1995**, *16*, 1170−1179.

(8) Svensson, M.; Humbel, S.; Froese, R.; Matsubara, T.; Sieber, S.; Morokuma, K. *J. Phys. Chem.* **1996**, *100*, 19357−19363.

(9) Humbel, S.; Sieber, S.; Morokuma, K. *J. Chem. Phys.* **1996**, *105*, 1959−1967.

(10) Dapprich, S.; Komaromi, K.; Byun, K.; Morokuma, K.; Frisch, M. *J. Mol. Struct. (THEOCHEM)* **1999**, *461*, 1−21.

(11) Vreven, T.; Morokuma, K. *J. Comput. Chem.* **2000**, *16*, 1419−1432.

(12) Vreven, T.; Mennucci, B.; daSilva, C.; Morokuma, K.; Tomasi, J. *J. Chem. Phys.* **2001**, *115*, 62−72.

(13) Vreven, T.; Morokuma, K. *Theor. Chem. Acc.* **2003**, *109*, 125−132.

(14) Ditchfield, R. *Mol. Phys.* **1974**, *27*, 789−807.

(15) Wolinski, K.; Hinton, J. F.; Pulay, P. *J. Am. Chem. Soc.* **1990**, *112*, 8251−8260 (and references therein).

(16) Gascon, J. A.; Batista, V. S. *Biophys. J.* **2004**, *87*, 2931−2941.

(17) Wald, G. *Science* **1968**, *162*, 230−239.

(18) Goldschmidt, C.; Ottolenghi, M.; Rosenfeld, T. *Nature* **1976**, *263*, 169−171.

(19) Rosenfeld, T.; Honig, B.; Ottolenghi, M.; Hurley, J.; Ebrey, T. *Pure Appl. Chem.* **1977**, *49*, 341−351.

(20) Honig, B.; Ebrey, T.; Callender, R.; Dinur, U.; Callender, R. *Proc. Natl. Acad. Sci. U.S.A.* **1979**, *76*, 2503−2507.

(21) Schoenlein, R.; Peteanu, L.; Mathies, R.; Shank, C. *Science* **1991**, *254*, 412−415.

(22) Wang, Q.; Schoenlein, R.; Peteanu, L.; Mathies, R.; Shank, C. *Science* **1994**, *266*, 422−424.

(23) Cooper, A. *FEBS Lett.* **1979**, *100*, 382−384.

(24) Cooper, A. *Nature* **1979**, *282*, 531−533.

(25) Schick, G.; Cooper, T.; Holloway, R.; Murray, L.; Birge, R. *Biochem.* **1987**, *26*, 2556−2562.

(26) Palczewski, K.; Kumasaka, T.; Hori, T.; Behnke, C.; Motoshima, H.; Fox, B.; Le Trong, I.; Teller, D.; Okada, T.; Stenkamp, R.; Yamamoto, M.; Miyano, M. *Science* **2000**, *289*, 739−745.

(27) Schertler, G.; Hargrave, P. *Methods Enzymol.* **2000**, *315*, 91−107.

(28) Teller, D.; Okada, T.; Behnke, C.; Palczewki, K.; Stenkamp, R. *Biochemistry* **2001**, *40*, 7761−7772.

(29) Okada, T.; Yoshinori, Y.; Silow, M.; Navarro, J.; Landau, J.; Schichida, Y. *Proc. Natl. Acad. Sci.* **2002**, *99*, 5982−5987.

(30) Okada, T.; Sugihara, M.; Bondar, A.; Elstner, M.; Entel, P.; Buss, V. *J. Mol. Biol.* **2004**, *342*, 571−583.

(31) Shriver, J. W.; Mateescu, G. D.; Abrahamson, E. W. *Biochemistry* **1979**, *18*, 4785−4792.

(32) Smith, S. O.; Palings, I.; Miley, M. E.; Courtin, J.; de Groot, H.; Lugtenburg, J.; Mathies, R. A.; Griffin, R. G. *Biochemistry* **1990**, *29*, 8158−8164.

(33) Smith, S. O.; Courtin, J.; de Groot, H.; Gebhard, R.; Lugtenburg, J. *Biochemistry* **1991**, *30*, 7409−7415.

(34) Wang, Q.; Kochendoerfer, G.; Schoenlein, R.; Verdegem, P.; Lugtenburg, J.; Mathies, R.; Shank, C. *J. Phys. Chem.* **1996**, *100*, 17388−17394.

(35) Feng, X.; Verdegem, P. J. E.; Lee, Y. K.; Sandström, D.; Edén, M.; Bovee-Geurts, P. H. M.; de Grip, W. J.; Lugtenburg, J.; Levitt, M. H. *J. Am. Chem. Soc.* **1997**, *119*, 6853−6857.

(36) Gröbner, G.; Choi, G.; Burnett, I. J.; Glaubitz, C.; Verdegem, P. J. E.; Lugtenburg, J.; Watts, A. *FEBS Lett.* **1998**, *422*, 201−204.

(37) Creemers, A. F. L.; Klaasen, C. H. W.; Bovee-Geurts, P. H. M.; Kelle, R.; Kragl, U.; Raap, J.; de Grip, W. J.; Lugtenburg, J.; de Groot, H. J. M. *Biochemistry* **1999**, *38*, 7195−7199.

(38) Verdegem, P. J. E.; Bovee-Geurts, P. H. M.; de Grip, W. J.; Lugtenburg, J.; de Groot, H. J. M. *Biochemistry* **1999**, *38*, 11316−11324.

(39) Feng, X.; Verdegem, P. J. E.; Eden, M.; Sandström, D.; Lee, Y. K.; Bovee-Geurts, P. H. M.; de Grip, W. J.; Lugtenburg, J.; de Groot, H. J. M.; Levitt, M. H. *J. Biomol. NMR* **2000**, *16*, 1−8.

(40) Gröbner, G.; Burnett, I. J.; Glaubitz, C.; Choi, G.; Mason, A. J.; Watts, A. *Nature* **2000**, *405*, 810−813.

(41) Verhoeven, M.; Creemers, A.; Bovee-Geurts, P. H. M.; deGrip, W.; Lugtenburg, J.; de Groot, H. J. M. *Biochemistry* **2001**, *40*, 3282−3288.

(42) Creemers, A. F. L.; Kiihne, S.; Bovee-Geurts, P. H. M.; DeGrip, W. J.; Lugtenburg, J.; de Groot, H. J. M. *Proc. Natl. Acad. Sci.* **2002**, *99*, 9101−9106.

(43) Carravetta, M.; Zhao, X.; Johannessen, O. G.; Lai, W. C.; Verhoeven, M. A.; Bovee-Geurts, P. H. M.; Verdegem, P. J. E.; Kiihne, S.; Luthman, H.; de Groot, H. J. M.; deGrip, W. J.; Lugtenburg, J.; Levitt, M. H. *J. Am. Chem. Soc.* **2004**, *126*, 3948−3953.

(44) Crocker, E.; Patel, A.; Eilers, M.; Jayaraman, S.; Getmanova, E.; Reeves, P.; Ziliox, M.; Khorana, H.; Sheves, M.; Smith, S. *J. Biomol. NMR* **2004**, *29*, 11−20.

(45) Fahmy, K.; Jäger, F.; Beck, M.; Zvyaga, T. A.; Sakmar, T. P.; Siebert, F. *Proc. Natl. Acad. Sci.* **1993**, *90*, 10206−10210.

(46) Fahmy, K.; Zvyaga, T.; Sakmar, T.; Siebert, F. *Biochemistry* **1996**, *35*, 15065−15073.

(47) Zvyaga, T.; Fahmy, K.; Siebert, F.; Sakmar, T. *Biochemistry* **1996**, *35*, 7536−7545.

(48) Deng, H.; Callender, R.; Rodman, H.; Honig, B. *Biophys. J.* **2001**, *51*, A268−A268.

(49) Eyring, G.; Curry, B.; Broek, A.; Lugtenburg, J.; Mathies, R. A. *Biochemistry* **1982**, *21*, 384−394.

(50) Palings, I.; Pardoen, J.; Van den Berg, E.; Winkel, C.; Lugtenburg, J.; Mathies, R. *Biochemistry* **1987**, *26*, 2544−2556.

(51) Lin, S. W.; Groesbeek, M.; van der Hoef, I.; Verdegem, P.; Lugtenburg, J.; Mathies, R. A. *J. Phys. Chem. B* **1998**, *102*, 2787−2806.

(52) Touw, S.; de Groot, H. J. M.; Buda, F. *J. Phys. Chem. B* **2004**, *108*, 13560−13572.

(53) Warshel, A.; Levitt, M. *J. Mol. Biol.* **1976**, *103*, 227−249.

(54) Karadakov, P.; Morokuma, K. *Chem. Phys. Lett.* **2000**, *317*, 589−596.

(55) Warshel, A.; Karplus, M. *J. Am. Chem. Soc.* **1974**, *96*, 5677−5689.

(56) Warshel, A. *Nature* **1976**, *260*, 679−683.

(57) Weiss, R.; Warshel, A. *J. Am. Chem. Soc.* **1979**, *101*, 6131−6133.

(58) Warshel, A.; Barboy, N. *J. Am. Chem. Soc.* **1982**, *104*, 1469−1476.

(59) Birge, R.; Hubbard, L. *J. Am. Chem. Soc.* **1980**, *102*, 2195−2205.

(60) Birge, R. *Annu. Rev. Biophys. Bioeng.* **1981**, *10*, 315−354.

(61) Birge, R.; Cooper, T. *Biophys. J.* **1983**, *42*, 61−69.

(62) Car, R.; Parrinello, M. *Phys. Rev. Lett.* **1985**, *55*, 2471−2474.

(63) Pastore, G.; Smargiassi, E.; Buda, F. *Phys. Rev. A* **1991**, *44*, 6334−6347.

(64) Tallent, J.; Hyde, E.; Findsen, L.; Fox, G.; Birge, R. *J. Am. Chem. Soc.* **1992**, *114*, 1581−1592.

(65) Bifone, A.; de Groot, H. J. M.; Buda, F. *J. Phys. Chem. B* **1997**, *101*, 2954−2958.

(66) Vreven, T.; Bernardi, F.; Garavelli, M.; Olivucci, M.; Robb, M.; Schlegel, H. B. *J. Am. Chem. Soc.* **1997**, *119*, 12687−12688.

(67) Garavelli, M.; Vreven, T.; Celani, P.; Bernardi, F.; Robb, M.; Olivucci, M. *J. Am. Chem. Soc.* **1998**, *120*, 1285−1288.

(68) La Penna, G.; Buda, F.; Bifone, A.; de Groot, H. J. M. *Chem. Phys. Lett.* **1998**, *294*, 447−453.

(69) Molteni, C.; Frank, I.; Parrinello, M. *J. Am. Chem. Soc.* **1999**, *121*, 12177−12183.

(70) Birge, R.; Vought, B. *Method. Enzymol.* **2000**, *315*, 143−163.

(71) Warshel, A.; Chu, Z. *J. Phys. Chem. B* **2001**, *105*, 9857−9871.

(72) Singh, D.; Hudson, B. S.; Birge, R. R. *Biochemistry* **2001**, *40*, 4201−4204.

(73) Rohrig, U.; Guidoni, L.; Rothlisberger, U. *Biochemistry* **2002**, *41*, 10799−10809.

(74) Saam, J.; Tajkhorshid, E.; Hayashi, S.; Schulten, K. *Biophys. J.* **2002**, *83*, 3097−3112.

(75) Furutani, Y.; Shichida, Y.; Kandori, H. *Biochemistry* **2003**, *42*, 9619−9625.

(76) Yamada, A.; Kakitani, T.; Yamamoto, S.; Yamato, T. *Chem. Phys. Lett.* **2002**, *366*, 670−675.

(77) Sugihara, M.; Buss, V.; Entel, P.; Elstner, M.; Frauenheim, T. *Biochemistry* **2002**, *41*, 15259−15266.

(78) Sugihara, M.; Entel, P.; Buss, V. *Phase Transit.* **2002**, *75*, 11−17.

(79) Ferre, N.; Olivucci, M. *J. Am. Chem. Soc.* **2003**, *125*, 6868−6869.

(80) Andruniow, T.; Ferre, N.; Olivucci, M. *Proc. Natl. Acad. Sci.* **2004**, *101*, 17908−17913.

(81) Ponder, J. W. *Tinker, version 3.9*; Washington University School of Medicine, St. Louis, MO, 2001.

(82) Sakmar, T.; Franke, R.; Khorana, H. *Proc. Natl. Acad. Sci. U.S.A.* **1989**, *86*, 8309−8313.

(83) Zhukovsky, E.; Oprian, D. *Science* **1989**, *246*, 928−930.

(84) Yan, E.; Kazmi, M.; De, S.; Chang, B.; Seibert, C.; Marin, E.; Mathies, R.; Sakmar, T. *Biochemistry* **2002**, *41*, 3620−3627.

(85) Birge, R. R.; Knox, B. E. *Proc. Natl. Acad. Sci.* **2003**, *100*, 9105−9107.

(86) Yan, E. C. Y.; Kazmi, M. A.; Ganim, Z.; Hou, J.; Pan, D.; Chang, B. S. W.; Sakmar, T. P.; Mathies, R. A. *Proc. Natl. Acad. Sci.* **2003**, *100*, 9262−9267.

(87) Frisch, M. J. et al. *Gaussian 03, Revision A.1*; Gaussian, Inc., Pittsburgh, PA, 2003.

(88) Ala-Laurila, P.; Donner, K.; Koskelainen, A. *Biophys. J.* **2004**, *86*, 3653−3662.

(89) Cornell, W. D.; Cieplak, P.; Bayly, C. I.; Gould, I. R.; Merz, K. M.; Ferguson, D. M.; Spellmeyer, D. C.; Fox, T.; Caldwell, J. W.; Kollman, P. A. *J. Am. Chem. Soc.* **1995**, *117*, 5179−5197.

(90) Wiberg, K. *J. Comput. Chem.* **1999**, *20*, 1299−1303.

(91) Helgaker, T.; Jaszuriski, M.; Ruud, K. *Chem. Rev.* **1999**, *99*, 293−352.

(92) Spooner, P. J. R.; Sharples, J. M.; Goodall, S. C.; Seedorf, H.; Verhoeven, M. A.; Lugtenburg, J.; Bovee-Geurts, P. H. M.; DeGrip, W. J.; Watts, A. *Biochemistry* **2003**, *42*, 13371−13378.

(93) Smith, S. O.; Palings, I.; Copie, V.; Raleigh, D.; Courtin, J.; Pardoen, J.; Lugtenburg, J.; Mathies, R.; Griffin, R. G. *Biochemistry* **1987**, *26*, 1606−1611.

(94) Tan, Q.; Lou, J.; Borhan, B.; Karnaukhova, E.; Berova, N.; Nakanishi, K. *Angew. Chem., Int. Ed. Engl.* **1997**, *36*, 2089−2093.

(95) Jäger, S.; Lewis, J.; Zvyaga, T.; Szundi, I.; Sakmar, T.; Kliger, D. *Proc. Natl. Acad. Sci.* **1997**, *94*, 8557−8562.

(96) Buss, V.; Kolster, K.; Terstegen, F.; Vahrenhorst, R. *Angew. Chem., Int. Ed. Engl.* **1998**, *37*, 18893−18895.

(97) Elstner, M.; Porezag, D.; Jungnickel, G.; Elsner, J.; Haugk, M.; Frauenheim, T.; Suhai, S.; Seifert, G. *Phys. Rev. B* **1998**, *58*, 7260−7268.

(98) MacKerell, A. D. et al. *J. Phys. Chem. B* **1998**, *102*, 3586−3616.

(99) Elia, G. R.; Childs, R. F.; Britten, J. F.; Yang, D. S. C.; Santarsiero, B. D. *Can. J. Chem.* **1996**, *74*, 591−601.

CT0500850